HHS Public Access

Author manuscript

Polyhedron. Author manuscript; available in PMC 2020 May 01.

Published in final edited form as:

Polyhedron. 2019 May 1; 163: 42–53. doi:10.1016/j.poly.2019.02.027.

Tetraazamacrocyclic derivatives and their metal complexes as antileishmanial leads

Timothy J. Hubin[1,*], **Ashlie N. Walker**[1], **Dustin J. Davilla**[1], **TaRynn N. Carder Freeman**[1], **Brittany M. Epley**[1], **Travis R. Hasley**[1], **Prince N. A. Amoyaw**[2], **Surendra Jain**[3], **Stephen J. Archibald**[4], **Timothy J. Prior**[4], **Jeanette A. Krause**[5], **Allen G. Oliver**[6], **Babu L. Tekwani**[3,7], and **M. Omar F. Khan**[2,8]

[1]Department of Chemistry and Physics, Southwestern Oklahoma State University. 100 Campus Drive, Weatherford, OK 73096

[2]Department of Pharmaceutical Sciences, College of Pharmacy, Southwestern Oklahoma State University. 100 Campus Drive, Weatherford, Ok 73096

[3]National Center for Natural Products Research and Department of BioMolecular Sciences, School of Pharmacy, University of Mississippi, University, MS 38677

[4]Department of Chemistry, University of Hull, Cottingham Road, Hull, HU6 7RX

[5]Department of Chemistry, University of Cincinnati, 301 Clifton Ct., Cincinnati, OH 45221-0172

[6]Department of Chemistry and Biochemistry, University of Notre Dame, Notre Dame, IN 46556

[7](Present address) Southern Research, Division of Drug Discovery, 2000 9th Avenue South Birmingham, AL 35205

[8](Present address) University of Charleston School of Pharmacy, 2300 MacCorkle Ave SE Charleston, WV 25304

Abstract

A total of 44 bis-aryl-monocyclic polyamines, monoaryl-monocyclic polyamines and their transition metal complexes were prepared, chemically characterized, and screened in vitro against the *Leishmania donovani* promastigotes, axenic amastigotes and intracellular amastigotes in THP1 cells. The IC_{50} and/or IC_{90} values showed that 10 compounds were similarly active at about 2-fold less potent than known drug pentamidine against promastigotes. The most potent compound had an IC_{50} of 2.82 μM (compared to 2.93 μM for pentamidine). Nine compounds were 1.1–13.6-fold

[*]Corresponding author. TJH: Tel.: +1 580 774 3026; fax: +1 580 774 3115; tim.hubin@swosu.edu.

Appendix A. Supplementary data

CCDC 1555221–1555225 contain the supplementary crystallographic data for [Cu(**L1**)Cl]PF_6, [Fe(**L3**)$(OAc)_2$], **L8**, [Ni(**L7**)(OAc)]PF_6. $(CH_3)_2CO$, and [Cu(**L10**)$(DMF)_2$]$(PF_6)_2$. 2DMF, respectively. These data can be obtained free of charge via http://www.ccdc.cam.ac.uk/conts/retrieving.html, or from the Cambridge Crystallographic Data Centre, 12 Union Road, Cambridge CB2 1EZ, UK; fax: (+44) 1223-336-033; or e-mail: deposit@ccdc.cam.ac.uk. Supplementary data to this article can be found online at https://doi.org/10.1016/j.poly.2019.02.027.

more potent than pentamidine against axenic amastigotes, the most potent one being about 2-fold less potent than amphotericin B. Fourteen compounds were about 2–10 fold more potent than pentamidine, the most potent one is about 2-fold less potent than amphotericin B against intracellular amastigotes in THP1 cells. The 2 most promising compounds (Fe**L7**Cl_2 and Mn**L7**Cl_2), with strong activity against both promastigotes and amastigotes and no observable toxicity against the THP1 cells are the Fe^{2+}- and Mn^{2+}- complexes of a dibenzyl cyclen derivative. Only 2 of the 44 compounds showed observable cytotoxicity against THP1 cells. Tetraazamacrocyclic monocyclic polyamines represent a new class of antileishmanial lead structures that warrant follow up studies.

Graphical Abstract:

Several bis-aryl-monocyclic polyamines and their metal complexes were shown to be potent in vitro inhibitors of *Leishmania donovani*. The synthesis of the two most promising compounds, Fe**L7**Cl_2 and Mn**L7**Cl_2, are shown below.

Keywords

Cyclen; cyclam; polyamine; antileishmanial drug lead; metal complexes

1. Introduction

Leishmaniasis, a vector born parasitic disease, affects 350 million people worldwide. Visceral leishmaniasis/kala azar (VL) is the most severe form resulting in 20,000 deaths every year. The other forms of leishmaniasis are cutaneous leishmaniasis (CL), mucocutaneous leishmaniasis (MCL), and post kala azar dermal leishmaniasis (PKDL).[1] One to two million new cases of the cutaneous form and half a million new cases of the visceral form occur each year. It is endemic in 98 countries, closely associated with poverty, with new cases mostly appearing in India, Bangladesh, Nepal, Brazil, Kenya, Sudan, and Ethiopia.[1,2] Multiple different morphological forms arise in the life cycles of *Leishmania*, differing mainly by the position, length and the cell body attachment of the flagellum.[3] Amastigotes are a typical morphology during an intracellular lifecycle stage in a human host. The promastigote form is a common morphology in the insect host. The extracellular form of *Leishmania* promastigotes is transmitted to humans through phlebotomine sandflies. The intracellular form of promastigotes replicates in the human host macrophages through a complicated life cycle.[3]

The currently available drugs for treatment of leishmaniasis are severely toxic, costly, or not effective due to increased resistance. The current first-line drug for treatment of visceral

leishmaniasis is pentavalent antimonial injections. The injections are inconvenient for therapies, lasting up to 21 days, since no oral forms of pentavalent antimonials are currently available. The use of pentavalent antimonials as first-line drugs for the past 70 years has led to resistance in many areas worldwide.[4–6] The second-line drug for therapy is amphotericin B, which requires a slow IV infusion and has severe side effects that can potentially be lethal.[5,6] Recent clinical trials have shown successful treatment of VL with a single dose of liposomal amphotericin B and combination therapies namely, amphotericB+ miltefosine, amphotericine B+paromomycin, miltefosine+ paromomycin and pentavalent antimonials+ paromomycin.[7]

The ability to metabolize polyamines is critical for *L. donovani* replication and survival. The enzymes associated with the pathway of polyamine biosynthesis and transport are promising targets for new antileishmanial drug discovery.[8–11] The critical enzymes in the metabolic pathway are ornithine decarboxylase (ODC), S-adenosylmethionine decarboxylase (AdoMetDC), spermidine synthase (SpdS), trypanothione synthetase (TryS), trypanothione reductase (TR) tryparedoxin peroxidase (TXNPx), deoxyhypusine synthase (DHS) and deoxyhypusine hydroxylase (DOHH).[9] Targeting these enzymes can potentially obstruct *L. donovani* replication. The inhibition of growth of *L. donovani* and *L. infantum* promastigotes in culture by difluoromethyl ornithine (DFMO),[12,13] an ODC inhibitor, was the first indication that polyamine biosynthesis is a potential drug target for leishmaniasis. Sing et al[14] has shown that the polyamine depletion due to the inhibition of ODC by 3-aminooxy-1-aminopropane (Fig. 1) is leishmanicidal. *Leishmania* parasites synthesize the polyamines putrescine and spermidine through the catalysis by ODC, AdoMetDC, and SpdS. Spermidine is utilized as a substrate to synthesize trypanothione for redox control. Trypanothione synthetase (TryS) and trypanothione reductase (TR) are two enzymes involved. Ullman and colleagues[15–17] have genetically validated all these enzymes as drug targets for *L. donovani*.

Several polyamine and oligoamine derivatives (Fig. 1) have been reported to have potent antileishmanial activity through the interference of polyamine biosynthetic enzymes or transport system.[18,19] CGP40215A and MDL73811 are potent inhibitors of AdoMetDC, which have been shown to inhibit growth of *L. donovani* promastigotes at micromolar concentration.[16,20] CGP40215A also inhibits growth of *L. donovani* amastigotes in mouse macrophages at concentrations up to 90 μM [59].[21] The polyamine analogue MDL27695 was shown to eliminate 77–100% of *L. donovani* amastigotes from mouse macrophages at a 1 μM concentration, possibly by interfering with DNA and RNA synthesis or inhibiting polyamine transport.[18,22] The oligoamines CGC-11211 and CGC-11226, and the macrocyclic polyamine analogue CGC-11235 showed potent antileismanial activity in vitro (IC_{50} < 1 μM), predominantly by interfering with the polyamine biosynthetic enzymes.[19] The polyamine-dependent redox metabolism including trypanothione as well as the polyamine transport mechanism have also been shown to be promising drug targets.[9,10,23–26]

In recent years there has been an increasing interest in the application of polyamines analogs and their transition metal complexes in medicine, including against malaria and leishmaniasis.[27–33] Several reports have shown that incorporation of transition metal ions into organic pharmacophores offer molecular diversity in drug discovery in addition to

enhancement of the biological activity.[34–36] The synthetic tetraazamacrocyclic compounds, particularly, cyclen and cyclam, and their analogs or their metal complexes have been extensively utilized in applications of a variety of diagnostic and magnetic resonance imaging (MRI) contrast agents.[37] Our group has extensively investigated tetraazamacrocycles and their metal complexes in drug discovery against variety of disease states including malaria, HIV, cancer, and schistosomiasis.[38–51] The facts that polyamine metabolism and related enzymes are established targets, and several oligoamine and polyamine derivatives have shown potent antileishmanial activity, triggered us to screen a set of tetraazamacrocyclic derivatives (Fig. 2) and their metal complexes against *L. donovani*, the causative agent for visceral leishmaniasis as an extension of our antiparasitic drug discovery initiatives.

2. Results and Discussion

2.1. Chemistry

All the ligands **L1–L10** in Figure 2 contain only one tetraazamacrocycle and different combinations of aromatic units for screening to determine which combination of groups maximizes antileishmanial efficacy. Ligands **L1** and **L2** contain one aromatic group, whereas **L3 – L10** contain two aromatic, or heteroaromatic groups. The tetraazamacrocyclic parent of **L1**, **L3-L7** is cyclen, whereas for **L2**, and **L8-L10 it** is cyclam.

2.1.1. Design Principles—The tetraazamacrocyclic ligands forming the foundation of this study have all been published over the past 20+ years (see experimental section for specific references). We selected a few structural types involving varying substitution patterns, including one, two, or three aromatic groups as a way to probe the importance of hydrophobicity to antileishmanial activity. We also chose to vary the bridging superstructure included on the macrocycle, from more flexible un-bridged, to short and rigid ethylene cross-bridged, to longer and less constrained propylene cross-bridged. The presence of the cross-bridge rigidifies the resulting transition metal complex, more fully engulfs the hydrophilic metal ion, and increases the kinetic stability of the metal complex compared to unbridged analogues.[52] If redox processes involving the metal ion of these complexes is involved in the antileishmanial activity, such stabilization would be important so that the potential drug molecule does not decompose upon oxidation/reduction.

Finally, we synthesized and screened complexes of the selected ligands with six different transition metal ions namely, Mn^{2+}, Fe^{2+}, Co^{2+}, Ni^{2+}, Cu^{2+} and Zn^{2+}. The biological significance of all of these metal ions are well-known. They are typically found in a variety of organisms, including humans, and are not expected to be toxic, particularly if bound strongly to a macrocyclic ligand. By producing metal complexes, we hoped to change the three-dimensional shape, hydrophobicity, and redox reactivity of the resulting potential drug leads. Choosing a range of metal ions allowed us to identify the metal complexes with the most potent antileishmanial activity. Establishing the properties of the most active metal ion complexes might help indicate the potential mechanism of action of the lead compounds against leishmania For example, Fe/Mn are known to have rich redox chemistries, while Zn is not.

2.1.2. Synthesis of ligands—A representative synthetic scheme for the benzyl substituted cyclam ligands is shown in Scheme 1. All of these ligands are previously published. Synthesis starting from cyclam proceeds through bis-aminals to give regioselective benzylation at non-adjacent nitrogens. Removal of the methylene aminal carbons yields **L10**,[53] which can be bridged by ditosyl propane to give **L9**.[54] Reductive ring cleavage by sodium borohydride of the dialkylated cyclam-glyoxal results in **L2**[49] and **L8**.[55] Analogous chemistry starting from cyclen results in **L1**,[51] **L3**,[55] **L4**,[56] and **L7**.[57]

The cyclen bisquinoline ligands **L5** and **L6** were prepared according to the synthetic route shown in Scheme 2.[39,47] The initial synthesis by direct derivatization using inorganic K_2CO_3 in DMF[39] was inefficient and the desired product (**L5**) was isolated in low yield (~35%). By choosing N-methylpyrrolidinone as the reaction solvent, with triethylamine as base, and elevating the reaction temperature, **L5** and **L6** were accessed in fair yields of up to 45%.[47]

2.1.3. Synthesis of transition metal complexes—Syntheses of Mn^{2+}, Fe^{2+}, Co^{2+}, Ni^{2+}, Cu^{2+} and Zn^{2+} complexes were attempted with **L1**-**L4** and **L7**-**L10** using anhydrous MCl_2 and/or $M(OAc)_2$ salts in anhydrous solvents such as MeOH, MeCN, and/or DMF (see Scheme 3). The products of complexations resulting in pure complexes are given in Table 1 and specific reaction conditions and basic characterization data are given in the Experimental Section. In general, unbridged tetraazamacrocycles (like **L7** and **L10**) can be complexed to metal ions in protic solvents like methanol without the ligand preferentially protonating from the solvent. However, in most cases, complexation to ethylene- and propylene-cross-bridged ligands (**L1**-**L4**, **L8**-**L9**) is most successful in aprotic solvents like acetonitrile or dimethylformamide where the highly basic proton sponge ligands are not protonated by solvent, which impedes metal ion complexation.[52] Complexations were generally carried out in an inert atmosphere glovebox to protect the metal ions from air oxidation and the ligands from protonation by water.[53] Not all complexations were successful, but a significant variety of complexes with different metal ion and ligand type were obtained to survey for antileishmanial activity among these tetraazamacroyclic ligands and complexes. Future work will include completing the full range of metal complexes for each ligand by finding successful reaction conditions for each metal-ligand pair. The reactions of $MnCl_2$ or $FeCl_2$ with ligand **L5** in a 1:1 ratio at 80°C for 1 week using DMF as a solvent in a glove box gave the complexes Mn(**L5**)Cl_2 and Fe(**L5**)(Cl_2, respectively in 45% and 29% yields, respectively.[50]

2.1.4. X-ray Crystallographic Structural Studies—In order to better understand the three dimensional structures of these potential drug molecules, and to correlate those structures with the biological activity observed, we have obtained a number of X-ray crystal structures. Not all ligands or metal complexes gave X-ray quality crystals, but we have obtained crystal structures of the following ligands, either alone or in a metal complex: **L1**, **L3**, **L7**, **L8**, and **L10**. We have also previously published additional X-ray crystal structures of metal complexes of **L2**,[49] **L3**,[58] and **L8**[48,51] which will be discussed. Tables containing data collection and refinement and metrical parameters for each structure are found in the electronic supplementary information.

[Cu(**L1**)Cl]PF_6 was prepared and crystallized (Fig. 3) as the acetate complex did not crystallize. In [Cu(**L1**)Cl]PF_6, the copper(II) center adopts a distorted square based pyramidal geometry. (Fig. 3a). The tetraazamacrocycle is forced into a folded (cis) arrangement by the ethyl bridge, and the ring nitrogens occupy three of the equatorial sites and the axial site, the typical coordination geometry for Cu^{2+} complexes of cross-bridged tetraazamacrocycles.[59,60,49,51–52] The single benzyl group is folded into the open coordination site of the five-coordinate Cu^{2+}, which is likely due to packing forces in the solid state, since no close interaction of the benzyl group with the metal ion is observed.[60] The previously published[49] structure of [Cu(**L2**)(OAc)]$^+$ (Fig. 3b) has an acetate bound to the Cu^{2+} center, and this bulky group causes the benzyl arm to be rotated away from the metal ion. This demonstrated flexibility may play a role in the antileishmanial activity discussed below.

[Mn(**L3**)Cl_2] (Fig. 4a) has previously been published,[58] but none of the other **L3** complexes screened here crystallized. However, the acetate precursor to [Fe(**L3**)(OAc)]PF_6, [Fe(**L3**)$(OAc)_2$], did form X-ray quality crystals (Fig. 4b).

Both structures have six-coordinate distorted octahedral coordination geometries around M^{2+} ions with folded, or cis, configurations of **L3** bonded by all four nitrogen atoms. [Mn(**L3**)Cl_2] has both benzyl groups rotated away from the Mn^{2+} ion and nearly coplanar (24.36° of their planes). However, in [Fe(**L3**)$(OAc)_2$], the benzyl group to rotate approximately perpendicular to the planes of the acetate carboxyl groups in order to fit between them in the solid state (65.26° of their planes). It remains to be determined if this flexibility plays a role in antileishmanial activity, or if the simple presence of two hydrophobic benzyl groups, regardless of flexibility, is all that is required for increased activity (*vide infra*).

No crystal structures for **L4-L6** or **L9** are known, according to the Cambridge Database (version 5.37) or grown by us. We include Cu(**CB3-DO2A**)$^+$ in figure (Fig. 5)[61] to demonstrate the similarity to ethylene cross-bridged complexes (**L1, L3** above) except for the 3-carbon cross-bridge, which makes the ligand cavity slightly larger and better able to encapsulate the metal ion (Cu^{2+} in this case). Obviously **L4**'s benzyl groups will not be coordinating, and we have demonstrated above how they would likely be arranged in complexes of **L4**. As dibenzyl compounds, some of the **L4** compounds demonstrate similar antileishmanial properties as the **L3** compounds (*vide infra*).

Neutral ligand **L8** itself, rather than a metal complex, crystallized from organic solvent. In aqueous solution, cross-bridged cyclams are proton sponges and are typically diprotonated.[62] In **L8**, the cross-bridge extends in front of the page (Fig. 6), showing the cavity for metal binding. Similarly to the [Fe(**L3**)$(OAc)_2$] complex, the benzyl rings are significantly non-planar (plane-plane angle of 54.00°). As will be discussed below, certain metal complexes of these ligands are typically more active against Leishmania than the free ligands themselves.

The final two X-ray crystal structures to be discussed are Ni(**L7**)$(OAc)^+$, which crystallized when the screened complex Ni(**L7**)Cl_2 did not, and Cu(**L10**)$(DMF)_2^{2+}$, which crystallized when the screened complex [Cu(**L10**)(OAc)]PF_6 did not (see Fig. 7).

These two crystal structure include, unlike any of those above, unbridged tetraazamacrocycles, and demonstrate the configurational flexibility of these ligands by producing both a folded (or cis) geometry (Ni(**L7**)$(OAc)^+$ (Fig. 7a) and a flat (or trans) geometry (Cu(**L10**)$(DMF)_2^{2+}$ (Fig. 7b)). A design principle (*vide supra*) used in producing this overall set of compounds for antileishmanial screening was to determine if the rigid, cross-bridged ligand complexes would be more or less active than the more flexible unbridged analogues. However, these two crystal structures clearly demonstrate the flexibility of the unbridged ligands. Not only are both cis and trans structures achieved, but the benzyl groups show even more rotational flexibility than seen in the cross-bridged structures discussed above. The plane-plane angle in Ni(**L7**)$(OAc)^+$ is 80.41°, the closest to perpendicular we have yet seen. While this plane-plane angle in Cu(**L10**)$(DMF)_2^{2+}$ is 0.00°, making them coplanar (this is also a required outcome of the crystallographic space group, P 2_1/n, where one half of the molecule is the asymmetric unit and generates the other. Both ligand **L7** and **L10** complexes are, in general, more active against leishmania than the cross-bridged ligands presented above. In fact, the Mn^{2+} and Fe^{2+} complexes of **L7** are identified as the most likely potential drug molecules identified in this study. Perhaps this is a result of the greater flexibility discussed above—a possibility that warrants further investigation.

2.2. Biological Evaluations of In vitro antileishmanial activity

2.2.1. Antileishmanial activity against promastigotes—

Ten compounds resulting from **L1–10** were significantly active to about 2-fold less potent than pentamidine against promastigotes. The IC_{50} values ranged from 2.82 to >20 μM compared to 2.93 μM for pentamidine (Table 1). The diaryl-monocyclic polyamine derivatives were more active than the monoaryl-monocyclic derivatives. For example, all of the monoaryl compounds' IC_{50}'s were >20 μM and were not further tested, while most of the diaryl compounds and/or their metal complexes showed IC_{50} values less than 20 μM. The most potent is a Mn^{2+}-complex of bisbenzyl cyclen derivative (**MnL7Cl$_2$**), which has an IC_{50} of 2.82 μM compared to 2.93 μM for pentamidine (Table 1). An Fe^{2+}-complex of cyclen bisquinoline (Fe**L5**Cl_2) was found to be most potent by IC_{90} values, with IC_{90} of 7.07 μM compared to 6.52 μM for pentamidine. However, this analog also showed IC_{50} and IC_{90} values of 3.95 and 8.79 μM, respectively against THP1 cells suggesting potential cytotoxicity. No simple conclusion regarding which metal ion (Mn^{2+}, Fe^{2+}, Co^{2+}, Ni^{2+}, Zn^{2+} and Cu^{2+}) best enhanced the antileishmanial activity over the parent ligands. However, it was generally observed that Mn^{2+}, Fe^{2+}, and Zn^{2+}-complexes were more potent than the corresponding free ligands, with Mn^{2+}-complexes typically being the most potent.

The three most potent ligands are **L3**, **L9** and **L10** with IC_{50} values 12.68, 12.98 and 9.40 μM; and IC_{90} values of 11.44, 18.97, and 17.84 μM, respectively (Table 1). Ligands **L3** is a dibenzyl ethyl cross-bridged cyclen, **L9** and **L10** are dibenzyl derivatives of cyclam (Fig. 2). The three most potent compounds against promastigotes are Mn**(L7)**Cl_2, Mn**(L9)**$MnCl_4$ and Fe**(L5)**Cl_2, among which only Mn**(L7)**Cl_2 has no toxicity against the THP1 cells, suggesting Mn**(L7)**Cl_2 as a lead for further study.

2.2.2. Antileishmanial activity against axenic amastigotes—

L. donovani promastigotes in culture have been transformed into potential amastigotes forms, which

normally grow intracellularly in the host macrophages. These culture-adapted forms are referred as axenic amastigotes and have been suggested as a useful model for in vitro antileishmanial screening and also for investigating mechanisms regulating the differentiation, survival and pathogenicity of the leishmania parasite.[63,64] Against axenic amastigotes, 9 compounds were 1.1–13.6-fold more potent than pentamidine, the most potent (Mn**L9**$MnCl_4$) being about 2-fold less potent than amphotericin B. This compound is also highly potent against promastigotes as well as intracellular amastigotes in THP1 cells. However, it is cytotoxic to the THP1 cells as mentioned above. Other compounds with reasonable activity against the axenic amastigotes are **L9** and all of its metal complexes, among which **L9** is the only other compound with comparable IC_{50} and IC_{90} values against THP1 cells as Mn**L9**MnCl4, again suggesting potential toxicity. Against intracellular amastigotes in THP1 cells, 14 compounds were about 2 to 10-fold more potent than pentamidine, the most potent (Mn**L7**Cl_2) is about 2-fold less potent than amphotericin B. This same compound was also found to be the most potent against promastigotes without sign of toxicity. The second most potent compound against the intracellular amastigotes in THP1 cells is Fe**(L7)**Cl_2, without sign of toxicity against the THP1 cells. This compound was also found to have good activity against promastigotes suggesting another potential lead for further study.

2.2.3. Summary of Biological Activity—In general, the diaryl compounds and their metal complexes (specifically Zn^{2+}, Fe^{2+}, or Mn^{2+} complexes) were found to be more potent compared to the monoaryl system possibly due to the higher lipophilicity and thus cell penetration. Two compounds with strong activity against both promastigotes and amastigotes and no observable toxicity against the THP1 cells are the Fe^{2+}- and Mn^{2+}-complexes of **L7**, a dibenzyl cyclen derivative (Fig. 2 and Table 1), which warrant further investigation.

The present study revealed several important findings. First, the diaryl monocyclic systems are more potent than monoaryl derivatives, perhaps due to more lipophilicity as well. Second, Fe^{2+}, and Mn^{2+} complexes increase the activity of both nonpolar and polar macrocyclic derivatives against both promastigotes and amastigotes of leishmanial parasites, although other metals also have inconsistently shown improvement in activity. Third, the polyamine ring systems are likely to be key structural targets for antileishmanial activity, as all the compounds showed reasonable growth inhibition of the leishmania parasites.

3. Conclusions

The results indicate that excellent antileishmanial potency can be obtained by transition metal complexation to tetraazamacrocycles. Interestingly, all of the most active compounds were transition metal complexes, not traditional “organic” compounds. The analogs with hydrophobic aryl rings showed higher antileishmanial potency, possibly due to improved cell permeability of these analogs. The improvement in the inhibitory potency beyond that of pentamidine required the complexation of Fe^{2+}, or Mn^{2+} and may indicate the role of polyamine biosynthesis and/or oxygen radicals formed by the redox cycling of ionic iron and manganese. It has previously been shown that several polyamines and oligoamines are potent growth inhibitors of leishmanial parasites through inhibition of ODC, AdoMetDC, or

polyamine transport system.[15,16] This study suggests the possible involvement of these compounds with interference of any of these enzymes in the polyamine biosynthetic pathway of leishmania parasites. Future detailed mechanistic and stability studies involving these ligands, and their metal complexes will be designed to unveil the role of complexed metal ions, especially iron, and manganese in antileishmanial activity. This study has laid a solid foundation towards the development of a new antileishmanial chemotherapy based on tetraazamacrocyclic derivatives and their metal complexes.

4. Experimental Section

4.1. Chemistry

4.1.1. General—All the materials were reagent grade, and used as supplied. The reactions were performed in anhydrous solvents under inert atmosphere unless otherwise indicated. Anhydrous solvents (acetonitrile and DMF) as well as all other reagents were used as received from a commercial source. Elemental analysis was carried out by Quantitative Technologies, Inc. in Whitehouse, NJ. Electrospray MS was obtained using a Shimadzu LCMS-2020 in 1:1 methanol/water mixture. ^{1}H and ^{13}C NMR spectra were recorded at 300 MHz and 75 MHz, respectively on Bruker 300 spectrometer with TMS as internal standard.

4.1.2. Synthesis of ligands and their Metal Complexes—Several ligands and their metal complexes were synthesized according to literature procedures: **L1**, [Cu(**L1**)(OAc)]PF_6, [Zn(**L3**)(OAc)]PF_6, [Zn(**L8**)(OAc)]PF_6, [Zn(**L2**)(OAc)]PF_6, [Cu(**L3**)(OAc)]PF_6, and [Zn(**L1**)(OAc)]PF_6;[51] **L2** and [Cu(**L2**)(OAc)]PF_6;[49] **L3**, **L8**,[55] and **L4**;[56] **L5**[39,47] Fe(**L5**)Cl_2 and Mn(**L5**)Cl_2;[50] **L6**[39,47], **L9**;[54] **L10**;[53] **L7** and;[57] [Fe(**L3**)Cl_2], [Mn(**L3**)Cl_2], [Mn(**L8**)Cl_2], and [Fe(**L8**)Cl_2][48]; [Ni(**8**)(OAc)]PF_6.48 Others were synthesized according to the following methods.

[Ni(**L2**)(OAc)]PF_6 • 0.35NH_4PF_6: (1.00 mmol, 0.331 g) of **L2** and 0.177 g (1.00 mmol) of anhydrous nickel(II) acetate were added to 25 ml of dry DMF in an inert atmosphere glovebox. The reaction was stirred at room temperature for 18 h. The crude [Ni(**L2**)(OAc)][(OAc)] solution was removed from the glovebox, filtered to remove any trace solids, and evaporated to dryness. The crude product was dissolved in 10 ml of dry methanol, to which was added dropwise a 5 ml dry methanol solution of 5 equivalents (0.815 g, 5.00 mmol) of NH_4PF_6. A pale purple powder precipitated, was collected, washed with cold methanol and ether, and dried under vacuum. Yield: 0.356 g (60%). Elemental analysis(%) calcd. [Ni($C_{20}H_{34}N_4$)($C_2H_3O_2$)]PF_6 • 0.35NH_4PF_6 (650.266 g/mol): C 40.64, H 5.95, N 9.37; Found C 40.46, H 5.70, N 9.59. MS (ES) *m/z* 447 [Ni(**L2**)(OAc)]$^+$.

[Ni(**L3**)(OAc)]PF_6: (1.00 mmol, 0.379 g) of **L3** and 0.177 g (1.00 mmol) of anhydrous nickel(II) acetate were added to 25 ml of dry DMF in an inert atmosphere glovebox. The reaction was stirred at room temperature for 18 h. The crude [Ni(**L3**)(OAc)][(OAc)] solution was removed from the glovebox, filtered to remove any trace solids, and evaporated to dryness. The crude product was dissolved in 10 ml of dry methanol, to which was added dropwise a 5 ml dry methanol solution of 5 equivalents (0.815 g, 5.00 mmols) of NH_4PF_6. A pale purple powder precipitated, was collected, washed with cold methanol and ether, and dried under vacuum. Yield: 0.414 g (67%). Elemental analysis (%) calcd. [Ni($C_{24}H_{34}N_4$)

$(C_2H_3O_2)]PF_6$ (641.260 g/mol): C 48.70, H 5.82, N 8.74; Found C 48.58, H 6.00, N 8.79. MS (ES) *m/z* 495 $[NiL(OAc)]^+$.

[Mn(**L4**)(OAc)]PF_6 • 1.9NH_4PF_6: (1.00 mmol, 0.392 g) of **L4** and 0.173 g (1.00 mmol) of anhydrous manganese(II) acetate were added to 10 ml of dry DMF in an inert atmosphere glovebox. The reaction was stirred at room temperature for 7 days, during which a white powder precipitated. This powder was filtered from solution and washed with minimal DMF and then diethyl ether before drying overnight open to the glovebox atmosphere. The white solid was then dissolved in 5 ml MeOH in the glovebox, and 5 equivalents (5.00 mmol, 0.815 g) of NH_4PF_6 dissolved in 3 ml MeOH was added, resulting in precipitation of the white powder product (0.194 g, 20%), which was filtered from solution and dried open to the glovebox atmosphere. Elemental analysis(%) calcd. $[Mn(C_{25}H_{36}N_4)(C_2H_3O_2)]PF_6$ • 1.9NH_4PF_6 (961.230 g/mol): C 33.74, H 4.89, N 8.60; Found C 33.58, H 5.03, N 8.39. MS (ES) *m/z* 445 [Mn(**L4**)]$^+$.

[Fe(**L4**)(OAc)]PF_6 • 1.2NH_4PF_6: (1.00 mmol, 0.392 g) of **L4** and 0.174 g (1.00 mmol) of anhydrous iron(II) acetate were added to 10 ml of dry DMF in an inert atmosphere glovebox. The reaction was stirred at room temperature for 7 days, during which a light brown powder precipitated. This powder was filtered from solution and washed with minimal DMF and then diethyl ether before drying overnight open to the glovebox atmosphere. The light brown solid was then dissolved in 5 ml MeOH in the glovebox, and 5 equivalents (5.00 mmol, 0.815 g) of NH_4PF_6 dissolved in 3 ml MeOH was added, resulting in precipitation of the light brown product (0.264 g, 31%), which was filtered from solution and dried open to the glovebox atmosphere. Elemental analysis(%) calcd. $[Fe(C_{25}H_{36}N_4)(C_2H_3O_2)]PF_6$ • 1.2NH_4PF_6 (848.040 g/mol): C 38.24, H 5.21, N 8.59; Found C 38.32, H 5.14, N 8.59. MS (ES) *m/z* 446 [Fe(**L4**)]$^+$.

[Co(**L4**)(OAc)]PF_6 • DMF: (1.00 mmol, 0.392 g) of **L4** and 0.177 g (1.00 mmol) of anhydrous cobalt(II) acetate were added to 10 ml of dry DMF in an inert atmosphere glovebox. The reaction was stirred at room temperature for 7 days, during which the solution became deep blue. The solution was removed from the glovebox, filtered to remove trace solids which were discarded, and the DMF was removed under vacuum. The deep purple oily solid remaining was then dissolved in 5 ml MeOH to give a pink solution, and 5 equivalents (5.00 mmol, 0.815 g) of NH_4PF_6 dissolved in 3 ml MeOH was added. This resulted in precipitation of the pink product (0.324 g, 44%), which was filtered from solution, washed with methanol and diethyl ether, and dried under vacuum. Elemental analysis(%) calcd. $[Co(C_{25}H_{36}N_4)(C_2H_3O_2)]PF_6$ • DMF (728.62 g/mol): C 49.45, H 6.36, N 9.61; Found C 49.77, H 6.12, N 9.25. MS (ES) *m/z* 452 [Co(**L4**)]$^+$.

[Zn(**L4**)(OAc)]PF_6 • 0.2DMF • 0.2H_2O: (1.00 mmol, 0.392 g) of **L4** and 0.183 g (1.00 mmol) of anhydrous zinc(II) acetate were added to 10 ml of dry DMF in an inert atmosphere glovebox. The reaction was stirred at room temperature for 7 days, during which the solution became orange. The solution was removed from the glovebox, filtered to remove trace solids which were discarded, and the DMF was removed under vacuum. The deep yellow solid remaining was then dissolved in 5 ml MeOH to give a yellow solution, and 5 equivalents (5.00 mmol, 0.815 g) of NH_4PF_6 dissolved in 3 ml MeOH was added. This resulted in

precipitation of the tan product (0.337 g, 49%), which was filtered from solution, washed with methanol and diethyl ether, and dried under vacuum. Elemental analysis (%) calcd. $[Zn(C_{25}H_{36}N_4)(C_2H_3O_2)]PF_6 \cdot 0.2DMF \cdot 0.2H_2O$ (683.82 g/mol): C 48.48, H 6.07, N 8.60; Found C 48.08, H 5.78, N 8.95. MS (ES) *m/z* 480 $[Zn(\mathbf{L4})Na]^+$.

$[Mn(\mathbf{L7})Cl_2]$: (1.00 mmol, 0.353 g) of **L7** and 0.126 g (1.00 mmol) of anhydrous manganese(II) chloride were added to 10 ml of dry DMF in an inert atmosphere glovebox. The reaction was stirred at room temperature for 7 days, during which a white powder formed. This solid was filtered off inside the glovebox, rinsed with diethyl ether, and allowed to dry open to the glovebox atmosphere to give the white powder product. Yield: 0.211 g (44%). Elemental analysis (%) calcd. $[Mn(C_{22}H_{32}N_4)Cl_2]$ (478.36 g/mol): C 55.24, H 6.74, N 11.71; Found C 55.10, H 6.51, N 11.58. MS (ES) *m/z* 455 $[Mn(\mathbf{L7})(MeOH)(OH)]^+$.

$[Fe(\mathbf{L7})Cl_2] \cdot 0.4DMF \cdot 0.5\ Et_2O$: (1.00 mmol, 0.353 g) of **L7** and 0.127 g (1.00 mmol)of anhydrous iron(II) chloride were added to 10 ml of dry DMF in an inert atmosphere glovebox. The reaction was stirred at room temperature for 7 days, during which a tan powder formed. This solid was filtered off inside the glovebox, rinsed with diethyl ether, and allowed to dry open to the glovebox atmosphere to give the white powder product. Yield: 0.228 g (42%). Elemental analysis (%) calcd. $[Fe(C_{22}H_{32}N_4)Cl_2] \cdot 0.4DMF \cdot 0.5\ Et_2O$ (545.57 g/mol): C 55.48, H 7.35, N 11.30; Found C 55.96, H 7.23, N 11.76. MS (ES) *m/z* 437 $[Fe(\mathbf{L7})(MeOH)]^+$; *m/z* 481 $[Fe(\mathbf{L7})Cl_2]^+$.

$[Ni(\mathbf{L7})Cl_2] \cdot 3H_2O$: (1.50 mmol, 0.529 g) of **L7** and 0.194 g (1.00 mmol) of anhydrous nickel(II) chloride were added to 15 ml of MeOH and 5 ml DMF. The reaction was heated to reflux with stirring under nitrogen for 3 days, during which a clear emerald green solution formed. The solution was cooled to room temperature, filtered to remove trace solids which were discarded, and evaporated to dryness forming a green oil. The oil was dissolved in 10 ml MeOH, to which 100 ml diethyl ether was added to precipitate out a green powder product. The green powder product was filtered, washed with diethyl ether, and dried under vacuum. Yield: 0.353 g (44%). Elemental analysis (%) calcd. $[Ni(C_{22}H_{32}N_4)Cl_2] \cdot 3H_2O$ (482.12 g/mol): C 49.28, H 7.14, N 10.45; Found C 49.23, H 7.08, N 10.30. MS (ES) *m/z* 447 $[Ni(\mathbf{L7})Cl]^+$.

$[Co(\mathbf{L8})(OAc)]PF_6 \cdot H_2O$: (1.00 mmol, 0.407 g) of **L8** and 0.177 g (1.00 mmol) of anhydrous cobalt(II) acetate were added to 25 ml of dry DMF in an inert atmosphere glovebox. The reaction was stirred at room temperature for 18 h. The crude $[Co(\mathbf{L7})(OAc)]$ [(OAc)] solution was removed from the glovebox, filtered to remove any trace solids, and evaporated to dryness. The crude products was dissolved in 10 ml of dry methanol, to which was added dropwise a 5 ml dry methanol solution of 5 equivalents (0.815 g, 5.00 mmols) of NH_4PF_6. A pale pink powder precipitated, was collected, washed with cold methanol and ether, and dried under vacuum. Yield: 0.416 g (60%). Elemental analysis (%) calcd. $[Co(C_{26}H_{38}N_4)(C_2H_3O_2)]PF_6 \cdot H_2O$ (687.572 g/mol): C 48.91, H 6.30, N 8.15; Found C 49.19, H 6.50, N 8.29. MS (ES) *m/z* 524 $[Co(\mathbf{L8})(OAc)]^+$.

[Mn(**L9**)][$MnCl_4$] • CH_3CN: (0.452 mmol, 0.190 g) of **L9** and 0.063 g (0.500 mmol) of anhydrous manganese(II) chloride were added to 5 ml of dry MeCN in an inert atmosphere glovebox. The reaction was stirred at room temperature for 7 days, during which a pale tan solution formed. This solution was filtered to remove trace solids, and evaporated to dryness under vacuum to give the pale tan powder product. Yield: 0.152 g (85% based on $MnCl_2$). Elemental analysis (%) calcd. [Mn($C_{27}H_{40}N_4$)][$MnCl_4$] • CH_3CN (713.37 g/mol): C 48.83, H 6.08, N 9.82; Found C 49.65, H 6.47, N 9.47. MS (ES) *m/z* 511 [Mn(**L9**)]$^+$.

[Fe(**L9**)][$FeCl_4$] • H_2O: (0.452 mmol, 0.190 g) of **L9** and 0.064 g (0.500 mmol) of anhydrous iron(II) chloride were added to 5 ml of dry MeCN in an inert atmosphere glovebox. The reaction was stirred at room temperature for 7 days, during which a brown solution formed. This solution was filtered to remove trace solids, and evaporated to dryness under vacuum to give the brown powder product. Yield: 0.137 g (79% based on $FeCl_2$). Elemental analysis (%) calcd. [Fe($C_{27}H_{40}N_4$)][$FeCl_4$] • H_2O (692.15 g/mol): C 46.85, H 6.11, N 8.10; Found C 46.97, H 5.71, N 7.85. MS (ES) *m/z* 512 [Fe(**L9**)]$^+$.

[Co(**L9**)$(OAc)_{1.1}$]$(PF_6)_{0.9}$ • DMF: (0.500 mmol, 0.211 g) of **L9** and 0.089 g (0.500 mmol) of anhydrous cobalt(II) acetate were added to 10 ml of dry DMF in an inert atmosphere glovebox and stirred overnight, forming a bright blue solution. The solution was removed from the glovebox, filtered to remove trace solids which were discarded, and evaporated to dryness forming a bright blue oil. The oil was dissolved in 7 ml dry MeOH, to which a 3 ml MeOH solution of 5 equivalents (2.50 mmol, 0.408 g) of NH_4PF_6 was added with stirring, and then stored overnight at −10 °C. The pink powder product was filtered, washed with methanol and diethyl ether, and dried under vacuum. Yield: 0.183 g (49%). [Co($C_{27}H_{40}N_4$)$(C_2H_3O_2)_{1.1}$]$(PF_6)_{0.9}$ • DMF (748.08 g/mol): C 51.70, H 6.78, N 9.36; Found C 51.61, H 7.09, N 9.37. MS (ES) *m/z* 557 [Co(**L9**)(OAc)(H_2O)]$^+$.

[Ni(**L9**)$(OAc)_{1.1}$]$(PF_6)_{0.9}$ • DMF: (0.500 mmol, 0.211 g) of **L9** and 0.089 g (0.500 mmol) of anhydrous nickel(II) acetate were added to 10 ml of dry DMF in an inert atmosphere glovebox and stirred overnight, forming a brown solution. The solution was removed from the glovebox, filtered to remove trace solids which were discarded, and evaporated to dryness forming a brown oil. The oil was dissolved in 5 ml dry MeOH, to which a 2 ml MeOH solution of 5 equivalents (2.50 mmol, 0.408 g) of NH_4PF_6 was added with stirring, and then stored overnight at −10 °C. The green powder product was filtered, washed with methanol and diethyl ether, and dried under vacuum. Yield: 0.154 g (41%). [Ni($C_{27}H_{40}N_4$)$(C_2H_3O_2)_{1.1}$]$(PF_6)_{0.9}$ • DMF (747.84 g/mol): C 51.72, H 6.78, N 9.36; Found C 51.49, H 6.98, N 9.45. MS (ES) *m/z* 595 [Ni(**L9**)$(OAc)_2$]$^+$.

[Zn(**L9**)(OAc)]PF_6 • $0.3NH_4PF_6$: (0.500 mmol, 0.211 g) of **L8** and 0.089 g (0.500 mmol) of anhydrous zinc(II) acetate were added to 10 ml of dry DMF in an inert atmosphere glovebox and stirred overnight, forming an orange solution. The solution was removed from the glovebox, filtered to remove trace solids which were discarded, and evaporated to dryness forming an orange oil. The oil was dissolved in 2 ml water, to which a 2 ml water solution of 5 equivalents (2.50 mmol, 0.408 g) of NH_4PF_6 was added with stirring, and then stored overnight at 5 °C. The brown sticky solid product was filtered, washed with methanol and diethyl ether, dissolved in 5 ml MeCN, and finally precipitated with 100 ml diethyl ether to

give a brown powder product, which was dried under vacuum. Yield: 0.150 g (41%). $[Zn(C_{27}H_{40}N_4)(C_2H_3O_2)](PF_6) \cdot 0.3NH_4PF_6$ (738.95 g/mol): C 47.14, H 6.03, N 8.15; Found C 47.25, H 6.03, N 8.12. MS (ES) *m/z* 547 $[Zn(\mathbf{L9})(OAc)]^+$.

$[Mn(\mathbf{L10})Cl_2] \cdot H_2O$: (1.00 mmol, 0.381 g) of **L10** and 0.126 g (1.00 mmol) of anhydrous manganese(II) chloride were added to 15 ml of dry MeOH in an inert atmosphere glovebox. The reaction was stirred at room temperature for 14 days, during which a white powder formed. This solid was filtered off inside the glovebox, and allowed to dry open to the glovebox atmosphere to give the white powder product. Yield: 0.307 g (59%). Elemental analysis (%) calcd. $[Mn(C_{24}H_{36}N_4)Cl_2] \cdot H_2O$ (524.43 g/mol): C 54.97, H 7.30, N 10.68; Found C 54.98, H 7.05, N 10.43. MS (ES) *m/z* 471 $[Mn(\mathbf{L10})Cl]^+$.

$[Fe(\mathbf{L10})Cl_2] \cdot 0.5H_2O$: (1.00 mmol, 0.381 g) of **L10** and 0.127 g (1.00 mmol) of anhydrous iron(II) chloride were added to 15 ml of dry MeOH in an inert atmosphere glovebox. The reaction was stirred at room temperature for 14 days, during which a white powder formed. This solid was filtered off inside the glovebox, and allowed to dry open to the glovebox atmosphere to give the off-white powder product. Yield: 0.283 g (55%). Elemental analysis (%) calcd. $[Fe(C_{24}H_{36}N_4)Cl_2] \cdot 0.5H_2O$ (516.33 g/mol): C 55.83, H 7.22, N 10.85; Found C 55.65, H 7.11, N 10.45. MS (ES) *m/z* 435 $[Fe(\mathbf{L19})]^+$; *m/z* 470 $[Fe(\mathbf{L9})Cl]^+$.

$[Co(\mathbf{L10})(OAc)](PF_6) \cdot H_2O$: 0.425 g (0.0011 mol) of 1,8-dibenzylcyclam and 0.195 g (0.0011 mol) of anhydrous cobalt(II) acetate were added to a 20 ml reaction vial in an inert atmosphere glovebox and 15 ml of anhydrous methanol was added. The reaction was stirred at room temperature for 7 days. The reaction vial was removed from the glovebox and the workup was done in air. The reaction solution was filtered through celite in a Pasteur pipette into a 100 mL roundbottom flask to remove any trace solids which were discarded. Separately, 5 equivalents (0.0055 mol, 0.897 g) of NH_4PF_6 was dissolved in a minimal amount of methanol (~5 ml) and added with stirring to the metal complex solution. A precipitate of the pink complex as a PF_6- salt formed immediately. The reaction flask was placed in a freezer (−10 °C) for 1 hour to complete the precipitation of the product. The solid pink powder product was collected on a fine glass frit, washed with a minimal amount of cold methanol, then ether. The pink powder product was transferred to a 4-dram vial and dried overnight under vacuum. Yield = 0.506 g (70%). $[Co(C_{24}H_{36}N_4)(C_2H_3O_2)](PF_6) \cdot H_2O$ (661.53 g/mol): C 47.21, H 6.25, N 8.47; Found C 47.45, H 6.07, N 8.53. MS (ES) *m/z* 470 $[Co(\mathbf{L10})(OAc)]^+$.

$[Cu(\mathbf{L10})](PF_6)_2 \cdot H_2O$: 0.425 g (0.0011 mol) of 1,8-dibenzylcyclam and 0.199 g (0.0011 mol) of anhydrous copper(II) acetate were added to a 20 ml reaction vial in an inert atmosphere glovebox and 15 ml of anhydrous methanol was added. The reaction was stirred at room temperature for 7 days. The reaction vial was removed from the glovebox and the workup was done in air. The reaction solution was filtered through celite in a Pasteur pipette into a 100 mL roundbottom flask to remove any trace solids which were discarded. Separately, 5 equivalents (0.0055 mol, 0.897 g) of NH_4PF_6 was dissolved in a minimal amount of methanol (~5 ml) and added with stirring to the metal complex solution. A precipitate of the bright blue complex as a PF_6- salt formed immediately. The reaction flask was placed in a freezer (−10 °C) for 1 hour to complete the precipitation of the product. The

solid bright blue powder product was collected on a fine glass frit, washed with a minimal amount of cold methanol, then ether. The bright blue powder product was transferred to a 4-dram vial and dried overnight under vacuum. Yield = 0.291 g (37%). $[Cu(C_{24}H_{36}N_4)](PF_6)_2 \cdot H_2O$ (752.06 g/mol): C 38.33, H 5.09, N 7.45; Found C 38.69, H 4.74, N 7.38. MS (ES) *m/z* 222 $[Cu(\mathbf{L10})]^{2+}$.

$[Zn(\mathbf{L10})(OAc)]PF_6 \cdot 0.1H_2O$: (1.00 mmol, 0.381 g) of **L10** and 0.183 g (1.00 mmol) of anhydrous zinc(II) acetate were added to 15 ml of dry MeOH in an inert atmosphere glovebox. The reaction was stirred at room temperature for 7 days, during which the solution became yellow. The solution was removed from the glovebox and filtered to remove trace solids, which were discarded. 5 equivalents (5.00 mmol, 0.815 g) of NH_4PF_6 dissolved in 3 ml MeOH was added. This resulted in precipitation of the tan product (0.176 g, 27%), which was filtered from solution, washed with methanol and diethyl ether, and dried under vacuum. Elemental analysis (%) calcd. $[Zn(C_{24}H_{36}N_4)(C_2H_3O_2)]PF_6 \cdot 0.1H_2O$ (651.79 g/mol): C 47.91, H 6.06, N 8.60; Found C 48.05, H 6.05, N 8.62. MS (ES) *m/z* 503 $[Zn(\mathbf{L10})(OAc)]^+$.

4.2. Biological evaluation

4.2.1. In vitro antileishmanial activity—The compounds were tested for different cellular forms of *L. donovani namely* promastigotes, axenic amastigotes and intracellular amastigotes in differentiated THP1 macrophages. These assays have been adapted to 384 well micro-plate format. A 3–4 days' old culture of *L. donovani* promastigotes or axenic amastigotes in the exponential phase was diluted with RPMI medium to 1×10^6 cells/ml for antileishmanial assays. The samples with appropriate dilutions were added to the promastigotes and axenic amastigotes cultures. The compounds were tested at six concentrations ranging from 10 to 0.0032 μg/ml. The plates were incubated at 26 °C for 72 hours (37 °C for axenic amastigotes) and growth of the parasites in cultures were determined by alamar Blue assay as described earlier.[65,66] The compounds were also tested against *L. donovani* intracellular amastigotes in THP1 cells employing a recently developed parasite-rescue and transformation assay.[67] The test samples were tested for cytotoxicity against THP1 cell cultures simultaneously. The conditions for seeding the THP1 cells, exposure to the test compounds and evaluation of cytotoxicity were the same as described in the parasite-rescue and transformation assay. IC_{50} and IC_{90} values were computed from the dose response curves usingXLFit®.

4.3. X-Ray Crystallography

Single crystal X-ray diffraction data were collected for NiL7 at beamline 11.3.1 at the Advanced Light Source (λ = 0.7749 Å), USA using a Bruker D8 diffractometer with PHOTON100 detector. The crystal was held at 150 K in an Oxford Cryosystems Cryostream Plus. Data were processed using Bruker APEX2 and SAINT[68] software and corrected for the effects of absorption by SADABS.[69] Single crystal X-ray diffraction data for all other structures were collected using a Stoe IPDS2 diffractometer with monochromated Mo Kα radiation (λ = 0.71073 Å). Crystals were held at 150 K in an Oxford Cryosystems Cryostream. Data were processed using Stoe X-AREA suit of programs. For FeL3 and CuL10 a multi-scan absorption correction was carried out within Sortav.[70] Crystal structures were solved using SHELXT (ref 3) and refined against all unique F2 values using SHELXL.

[71] Hydrogen atoms were added at geometrically calculated positions except in the case of those attached to nitrogen or oxygen, for which atom positions were refined subject to chemically-sensible restraints.

Supplementary Material

Refer to Web version on PubMed Central for supplementary material.

Acknowledgement

This work was supported by the National Institute of General Medical Sciences of the National Institutes of Health [grant number 8P20GM103447]; Research Corporation [CC6505]; the Oklahoma Center for the Advancement of Science and Technology [HR13–157]; the Stephenson Cancer Center [Experimental Therapeutics Seed Grant]; and the Henry Dreyfus Teacher-Scholar Awards Program (TJH). The NCNPR biological screening activities are partly supported by the USDA-ARS Cooperative Scientific Agreement No. 58-6408-2-0009 and National Center for Natural Products Research, University of Mississippi. Some crystallographic data were collected through the SCrALS (Service Crystallography at Advanced Light Source) program at the Small-Crystal Crystallography Beamline 11.3.1 at the Advanced Light Source (ALS), Lawrence Berkeley National Laboratory. The ALS is supported by the U.S. Department of Energy, Office of Energy Sciences Materials Sciences Division, under contract DE-AC02–05CH11231.

References

1. Nagle AS, Khare S, Kumar AB, Supek F, Buchynskyy A, Mathison CJN, Chennamaneni NK, Pendem N, Buckner FS, Gelb MH, Molteni V. Recent developments in drug discovery for leishmaniasis and human African trypanosomiasis. Chem Rev 2014;114(22):11305–11347. [PubMed: 25365529]
2. Chappuis F, Sundar S, Hailu A, Ghalib H, Rijal S, Peeling RW, Alvar J, Boelaert M. Visceral leishmaniasis: what are the needs for diagnosis, treatment and control? Nat Rev Microbiol 2007;5(11):873–82. [PubMed: 17938629]
3. Berman J Visceral leishmaniasis in the New World & Africa. Indian J Med Res 2006;123:289–294. [PubMed: 16778311]
4. Croft SL, Sundar S, Fairlamb AH. Drug resistance in leishmaniasis. Clin Microbiol Rev 2006;19(1): 111–26. [PubMed: 16418526]
5. Kedzierski L, Sakthianandeswaren A, Curtis JM, Andrews PC, Junk PC, Kedzierska K. Leishmaniasis: Current Treatment and Prospects for New Drugs and Vaccines. Curr Med Chem 2009;16:599–614. [PubMed: 19199925]
6. Moore EM, Lockwood DN. Treatment of visceral leishmaniasis. J Glob Infect Dis 2010;2:151–158. [PubMed: 20606971]
7. Sundar S, Singh A. Recent developments and future prospects in the treatment of visceral leishmaniasis. Ther Adv Infect Dis 2016;3(3–4):98–109. [PubMed: 27536354]
8. Heby O, Persson L, Rentala M. Chagas' disease, and leishmaniasis. Amino Acids 2007;33:359–366. [PubMed: 17610127]
9. Ilari A, Fiorillo A, Baiocco P, Poser E, Angiulli G, Colotti G.. Targeting polyamine metabolism for finding new drugs against leishmaniasis: A review. Mini Rev Med Chem 2015;15(3):243–252. [PubMed: 25769972]
10. Kandpal M, Tekwani BL. Polyamine transport systems of *Leishmania donovani* promastigotes. Life Sci 1997;60:1793–1802. [PubMed: 9150419]
11. Reguera RM, Tekwani BL, Balaña-Fouce R. Polyamine transport in parasites: a potential target for new antiparasitic drug development. Comp Biochem Physiol C Toxicol Pharmacol 2005;140(2): 151–164. [PubMed: 15907761]
12. Kaur K, Emmett K, McCann PP, Sjoerdsma A, Ullman B. Effects of DL-α-difluoromethylornithine on Leishmania donovani promastigotes. J Protozool 1986:33:518–521. [PubMed: 3098971]

13. Balana-Fouce R, Ordonez D, Alunda JM. Putrescine transport system in *Leishmania infantum* promastigotes. Mol Biochem Parasitol 1989;35:43–50. [PubMed: 2503722]
14. Singh S, Mukherjee A, Khomutov AR, Persson L, Heby O, Chatterjee M, Madhubala R. Antileishmanial effect of 3-aminooxy-1-aminopropane is due to polyamine depletion. Antimicrob Agents Chemother 2007;51(2):528–534. [PubMed: 17101681]
15. Roberts SC, Jiang Y, Jardim A, Carter NS, Heby O, Ullman B. Genetic analysis of spermidine synthase from Leishmania donovani. Mol Biochem Parasitol 2001;115:217–226. [PubMed: 11420108]
16. Roberts SC, Scott J, Gasteier JE, Jiang Y, Brooks B, Jardim A, Carter N,S; Heby O, Ullman B. S-adenosylmethionine decarboxylase from Leishmania donovani. Molecular, genetic, and biochemical characterization of null mutants and overproducers. J Biol Chem 2002;277:5902–5909. [PubMed: 11734561]
17. Jiang Y; Roberts SC; Jardim A; Carter NS; Shih S; Ariyanayagam M; Fairlamb AH; Ullman B Ornithine decarboxylase gene deletion mutants of Leishmania donovani. J Biol Chem 1999;274:3781–3788. [PubMed: 9920931]
18. Birkholtz L-M, Williams M, Niemand J, Louw AI, Persson L, Heby O. Polyamine homoeostasis as a drug target in pathogenic protozoa: peculiarities and possibilities Biochem. J 2011;438:229–244. [PubMed: 21834794]
19. Roberts SC, Jiang Y, Gasteier J, Frydman B, Marton LJ, Heby O, Ullman B. *Leishmania donovani* polyamine biosynthetic enzyme overproducers as tools to investigate the mode of action of cytotoxic polyamine analogs. Antimicrob. Agents Chemother 2007;51:438–445. [PubMed: 17116678]
20. Mukhopadhyay R, Kapoor P, Madhubala R. Antileishmanial effect of a potent S-adenosylmethionine decarboxylase inhibitor: CGP 40215A. Pharmacol Res 1996;33:67–70. [PubMed: 8817649]
21. Brun R, Bühler Y, Sandmeier U, Kaminsky R, Bacchi CJ, Rattendi D, Lane S, Croft SL, Snowdon D, Yardley V. In vitro trypanocidal activities of new S-adenosylmethionine decarboxylase inhibitors. Antimicrob Agents Chemother 1996;40:1442–1447. [PubMed: 8726017]
22. Baumann RJ, Hanson WL, McCann PP, Sjoerdsma A, Bitonti AJ. Suppression of both antimony-susceptible and antimony-resistant *Leishmania donovani* by a bis(benzyl)polyamine analog. Antimicrob Agents Chemother 1990;34:722–727. [PubMed: 2360812]
23. Krauth-Siegel RL; Inhoff O Parasitol. Res 2003, 90(spl2), S77. [PubMed: 12709793]
24. Khan MOF. Trypanothione Reductase: A Viable Chemotherapeutic Target for Antitrypanosomal and Antileishmanial Drug Design Drug Target Insights 2007;2:129–146. [PubMed: 21901070]
25. Fyfe PK, Oza SL, Fairlamb AH, Hunter WN. Leishmania trypanothione synthetaseamidase structure reveals a basis for regulation of conflicting synthetic and hydrolytic activities. J Biol Chem 2008;283:17672–17680. [PubMed: 18420578]
26. Basselin M, Coombs GH, Barrett MP. Putrescine and spermidine transport in *Leishmania*. Mol. Biochem. Parasitol 2000;109:37–46. [PubMed: 10924755]
27. Caminos AP, Panozzo-Zenere EA, Wilkinson SR, Tekwani BL, Labadie GR. Synthesis and antikinetoplastid activity of a series of N,N'-substituted diamines. Bioorg Med Chem Lett 2012;22:1712–1715. doi: 10.1016/j.bmcl.2011.12.101 [PubMed: 22248858]
28. Gasser G, Metzler-Nolte N. In: Alessio E, ed. Bioinorganic Medicinal Chemistry; Weinheim: Wiley-VCH;2011:351–382.
29. Hernandes MZ, Pontes FJS, Coelho LCD, Moreira DRM, Pereira VRA, Leite ACL. Recent insights on the medicinal chemistry of metal-based compounds: hints for the successful drug design. Curr Med Chem 2010;17:3739–3750. [PubMed: 20846108]
30. Arrowsmith RL, Pascu SI, Smugowski H. New developments in the biomedical chemistry of metal complexes: from small molecules to nanotheranostic design. Organomet Chem 2012;38:1–35. DOI: 10.1039/9781849734868-00001.
31. Hartinger CG, Metzler-Nolte N, Dyson PJ. Challenges and opportunities in the development of organometallic anticancer drugs. Organometallics 2012;31:5677–5685.

32. Jagu E, Djilali R, Pomel S, Ramiandrasoa F, Pethe S, Labruere R, Loiseau P. M, Blonski C. Design, synthesis and in vitro antikinetoplastid evaluation of N-acylated putrescine, spermidine and spermine derivatives. Bioorg Med Chem Lett 2015;25(2): 207–209. [PubMed: 25499437]
33. Salamana RX, Salgueiro CM, Forest CO, Casadevall CA, Fillol LJ, Moreno SM, Sanchez MC, Lombardo RMJ, Arevalo OF. Patent No. ES 2440896A1;1 30, 2014:WO 2015059337A1, Spanish, Apr 30;2015.
34. Jones C, Thornback J. Chapter 4: Therapeutic Medicine In: Jones CJ, Thornback J, eds. Medicinal Application of Coordination Chemistry Cambridge, UK: Royal Society of Chemistry,2007:201–321.
35. Aird RE, Cummings J, Ritchie AA, Muir M, Morris RE, Chen H, Sadler PJ, Jodrell DI. In vitro and in vivo activity and cross resistance profiles of novel ruthenium (II) organometallic arene complexes in human ovarian cancer. Br J Cancer 2002;86:1652–1657. [PubMed: 12085218]
36. Bahl D, Athar F, Soares MBP, Santos de Sa M, Moreira DRM, Srivastava RM, Leite ACL, Azam A. Structure–activity relationships of mononuclear metal–thiosemicarbazone complexes endowed with potent antiplasmodial and antiamoebic activities. Bioorg Med Chem 2010;18:6857–6864. [PubMed: 20719524]
37. Baker WC, Choi MJ, Hill DC, Thompson JL, Petillo PA. Synthesis of lipophilic paramagnetic contrast agents J Org Chem 1999;64:2683–2689. [PubMed: 11674337]
38. Hubin TJ, Amoyaw PNA, Roewe KD, Simpson NC, Maples RD, Freeman TNC, Cain AN, Le JG, Archibald SJ, Khan SI, Tekwani BL, Khan MOF. Synthesis and antimalarial activity of metal complexes of cross-bridged tetraazamacrocyclic ligands. Bioorg Med Chem 2014;22:3239–3244. [PubMed: 24857776]
39. Khan MOF, Levi MS, Tekwani BL, Khan SI, Kimura E, Borne RF. Synthesis and antimalarial activities of cyclen 4-aminoquinoline analogs. Antimicrob Agents Chemother 2009;53(4):1320–1324. [PubMed: 19171802]
40. Khan A, McRobbie G, Madden LA, Empson CJ, Bridgeman AJ, Ullom R, Hubin TJ, Greenman J, Archibald SJ. Configurationally restricted bis-azamacrocycles: chemokine receptor antagonists. Immunol 2005;116:75.
41. Valks GC, McRobbie G, Lewis EA, Hubin TJ, Hunter TM, Sadler PJ, Pannecouque C, De Clerq E, Archibald SJ. Configurationally-restricted bismacrocyclic CXCR4 receptor antagonists. J Med Chem 2006;49:6162–6165. [PubMed: 17034122]
42. Archibald SJ, Daelemans D, Hubin TJ, Huskens D, Schols D, Van Laethem K, De Clercq E, Pannecouque C. CXCR4 Chemokine Receptor Antagonists from Ultra-rigid Metal Complexes Profoundly Inhibit HIV-1 Replication, and also AMD3100-resistant Strains. Antiviral Res 2009;82:A45.
43. Khan A, Nicholson G, McRobbie G, Greenman J, Pannecouque C, Daelemans D, Schols D, De Clercq E, Hubin TJ, Archibald SJ. CXCR4 Antagonists: A New Generation of Configurationally Restricted Bis-azamacrocyclic Compounds. Antiviral Res 2009;82:A59.
44. Timmons JC, Hubin TJ. Preparations and Applications of Synthetic Linked Azamacrocycle Ligands and Complexes. Coord Chem Rev 2010;254:1661–1685.
45. Panneerselvam J, Jin J, Shanker M, Lauderdale J, Bates J, Wang Q, Khan A, Hubin TJ, Archibald SJ, Ramesh R. IL-24 prevents lung cancer cell migration and invasion by disrupting the SDF-1a/CXCR4 signaling axis. PLOS One, 2015;10:0122439.
46. Rudraraju AV, Amoyaw PNA, Hubin TJ, Khan MOF. Determination of log P values of new cyclen based antimalarial drug leads using RP-HPLC. Pharmazie 2014;69:655–662. [PubMed: 25272935]
47. Amoyaw PA, Pham K, McClain JM, Cain AN, Hubin TJ, Khan MOF. Synthesis of novel tetraazamacrocyclic bisquinoline derivatives as potential antimalarial agents. Curr Org Synth 2014;11:916–921.
48. Smith R, Huskens D, Daelemans D, Mewis RE, Garcia CD, Cain AN, Carder Freeman TN, Pannecouque C, De Clercq E, Schols D, Hubin TJ, Archibald SJ. Metal ion containing CXCR4 chemokine receptor antagonists: nickel(II) complexes of configurationally restricted macrocycles. Dalton Trans, 2012;41:11369–11377. [PubMed: 22892890]
49. Khan A, Nicholson G, Greenman J, Madden L, McRobbie G, Pannecouque C, De Clercq E, Silversides JD.; Ullom R, Maples DL, Maples RD, Hubin TJ, Archibald SJ. Binding optimization

through coordination chemistry: fixed geometry CXCR4 chemokine receptor antagonists from ultra rigid metal complexes. J Am Chem Soc 2009;131:3416–3417. [PubMed: 19231846]

50. Khan MOF, Keiser J, Amoyaw PNA, Hossain MF, Vargas M, Le JG, Simpson NC, Roewe KD, Freeman TNC, Hasley TR, Maples RD, Archibald SJ, Hubin TJ. Discovery of antischistosomal drug leads based on tetraazamacrocyclic derivatives and their metal complexes. Antimicrob Agents Chemother 2016;60:5331–5336. doi:10.1128/AAC.00778-16. [PubMed: 27324765]
51. Maples RD, Cain AN, Burke BP, Silversides JD, Mewis R, D'huys T, Schols D, Linder DP, Archibald SJ, Hubin TJ. Aspartate-based CXCR4 receptor binding of cross-bridged tetraazamacrocyclic copper(II) and zinc(II) complexes. Chem Eur J 2016;22:12916–12930. DOI: 10.1002/chem.201601468. [PubMed: 27458983]
52. Hubin TJ. Synthesis and coordination chemistry of topologically constrained azamacrocycles. Coord Chem Rev 2003;241:27–46.
53. Royal G, Dahaoui-Gindrey V, Dahaoui S, Tabard A, Guilard R, Pullumbi P, Lecomte C. New synthesis of trans-disubstituted cyclam macrocycles—elucidation of the disubstitution mechanism on the basis of x-ray data and molecular modeling. Eur J Org Chem 1998;1998:1971–1975.
54. Dale AV; An GI; Pandya DN; Ha YS; Bhatt N; Soni N; Lee H; Ahn H; Sarkar S; Lee W; Huynh PT; Kim JY; Gwon M-R; Kim SH; Park JG; Yoon Y-R; Yoo JS Inorg Chem, 2015, 54, 8177–8186. [PubMed: 26286436]
55. Weisman GR, Wong EH, Hill DC, Rogers ME, Reed DP, Calabrese JC. Synthesis and transition-metal complexes of new cross-bridged tetraamine ligands. Chem Commun 1996;1996:947–948.
56. Yoo JS, Darpan P. PCT Int Appl 2011;WO 2011031073 A2 20110317.
57. a)Averin AD, Shukhaev AV, Buryak AK, Denat F, Guilard R, Beletskaya IP. Synthesis of a new family of bi- and polycyclic compounds via Pd-catalyzed amination of 1,7-di(3-bromobenzyl)cyclen. Tetrahedron Lett 2008;49:3950–3954.b)Oukhatar F, Beyler M, Tripier R. Straightforward and mild deprotection methods of N-mono- and N1,N7-functionalised bisaminal cyclens. Tetrahedron 2015;71:3857–3862.
58. Hubin TJ, McCormick JM, Collinson SR, Alcock NW, Clase HJ, Busch DH. Synthesis and X-ray crystal structures of iron(II) and manganese(II) complexes of unsubstituted and benzyl substituted cross-bridged tetraazamacrocycles Inorg Chim Acta 2003;346:76–86.
59. Hubin TJ, McCormick JM, Alcock NW, Clase HJ, Busch DH. Crystallographic characterization of stepwise changes in ligand conformations as their internal topology changes, and two novel cross-bridged tetraazamacrocycle copper(II) complexes. Inorg. Chem, 1999, 38, 4435. [PubMed: 11671154]
60. Hubin TJ, Alcock NW, Busch DH. Cu(I) and Cu(II) complexes of an ethylene cross-bridged cyclam. Acta Cryst. C, 2000, 56, 37. [PubMed: 10710660]
61. Odendaal AY, Fiamengo AL, Ferdani R, Wadas TJ, Hill DC, Peng Y, Heroux KJ, Golen JA, Rheingold AL, Anderson CJ, Weisman GR, Wong EH. Isomeric Trimethylene and Ethylene Pendant-armed Cross-bridged Tetraazamacrocycles and in Vitro/in Vivo Comparisions of their Copper(II) Complexes. Inorg. Chem 2011, 50, 3078–3086. [PubMed: 21381676]
62. Weisman GR, Rogers ME, Wong EH, Jasinski JP, Paight ES. Cross-Bridged Cyclam. Protonation and Li Complexation in a Diamond-Lattice Cleft. J. Am. Chem. Soc, 1990, 112, 8604–8605.
63. Gupta N, Goyal N, Rastogi AK. In vitro cultivation and characterization of axenic amastigotes of Leishmania. Trends Parasitol 2001;17(3):150–153. [PubMed: 11286801]
64. Pan AA, Duboise SM, Eperon S, Rivas L, Hodgkinson V, Traub-Cseko Y, McMahon-Pratt D. Developmental life cycle of Leishmania – cultivation and characterization of cultured extracellular amastigotes. J Eukaryot Microbiol 1993;40(2):213–223. [PubMed: 8461895]
65. Rahman AA, Samoylenko V, Jacob MR, Sahu R, Jain SK, Khan SI, Tekwani BL, Muhammad I. Antiparasitic and antimicrobial indolizidines from the leaves of *Prosopis glandulosa var. glandulosa*. Planta Med 2011;77(14):1639–43. [PubMed: 21384317]
66. Manda S, Khan SI, Jain SK, Mohammed S, Tekwani BL, Khan IA, Vishwakarma RA, Bharate SB Synthesis, antileishmanial and antitrypanosomal activities of N-substituted tetrahydro-β-carbolines. Bioorg Med Chem Lett 2014;24(15):3247–50. [PubMed: 24980054]
67. Jain SK, Sahu R, Walker LA, Tekwani BL. A parasite rescue and transformation assay for antileishmanial screening against intracellular Leishmania donovani amastigotes in THP1 human

acute monocytic leukemia cell line. J Vis Exp2012;(70):4054. doi: 10.3791/4054. [PubMed: 23299097]

68. Bruker (2012). APEX2, SAINT Bruker AXS Inc., Madison, Wisconsin, USA
69. Bruker (2001). SADABS Bruker AXS Inc., Madison, Wisconsin, USA.
70. Blessing RH (1995). An Empirical Correction for Absorption Anisotropy. Acta Cryst. A 51, 33–38. [PubMed: 7702794]
71. Sheldrick GM (2015). Acta Cryst C71, 3–8.

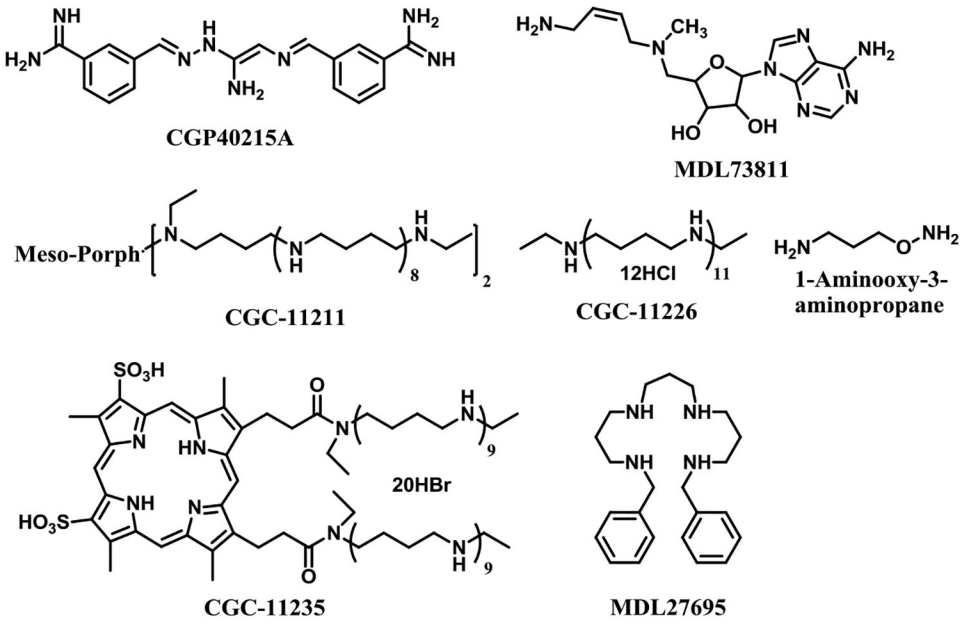

Figure 1.

Representative structures of polyamine and oligoamine derivatives reported to have potent antileishmanial activity.[18,19]

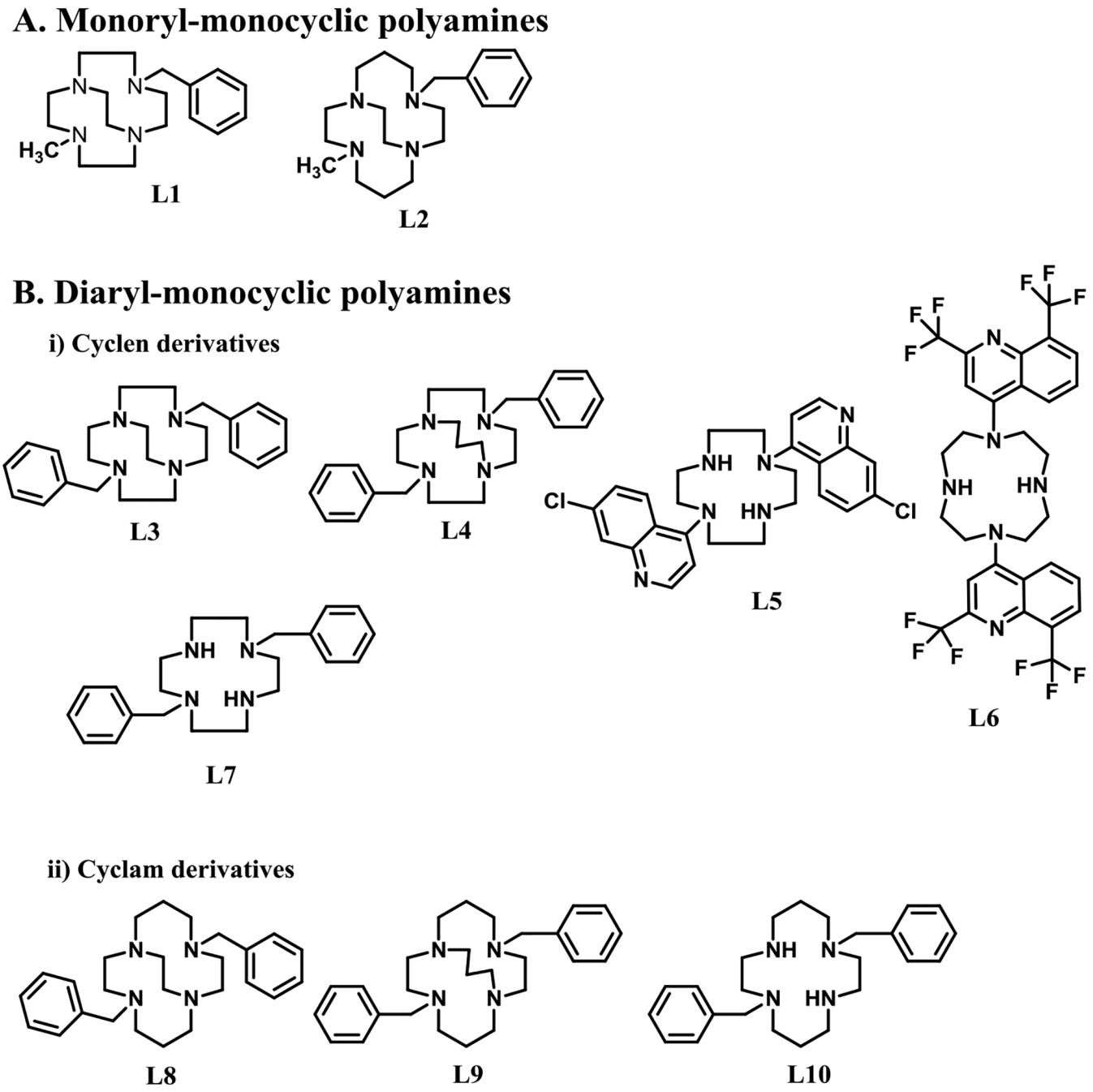

Figure 2.
Structures of the tetraazamacrocyclic ligands used in this study.

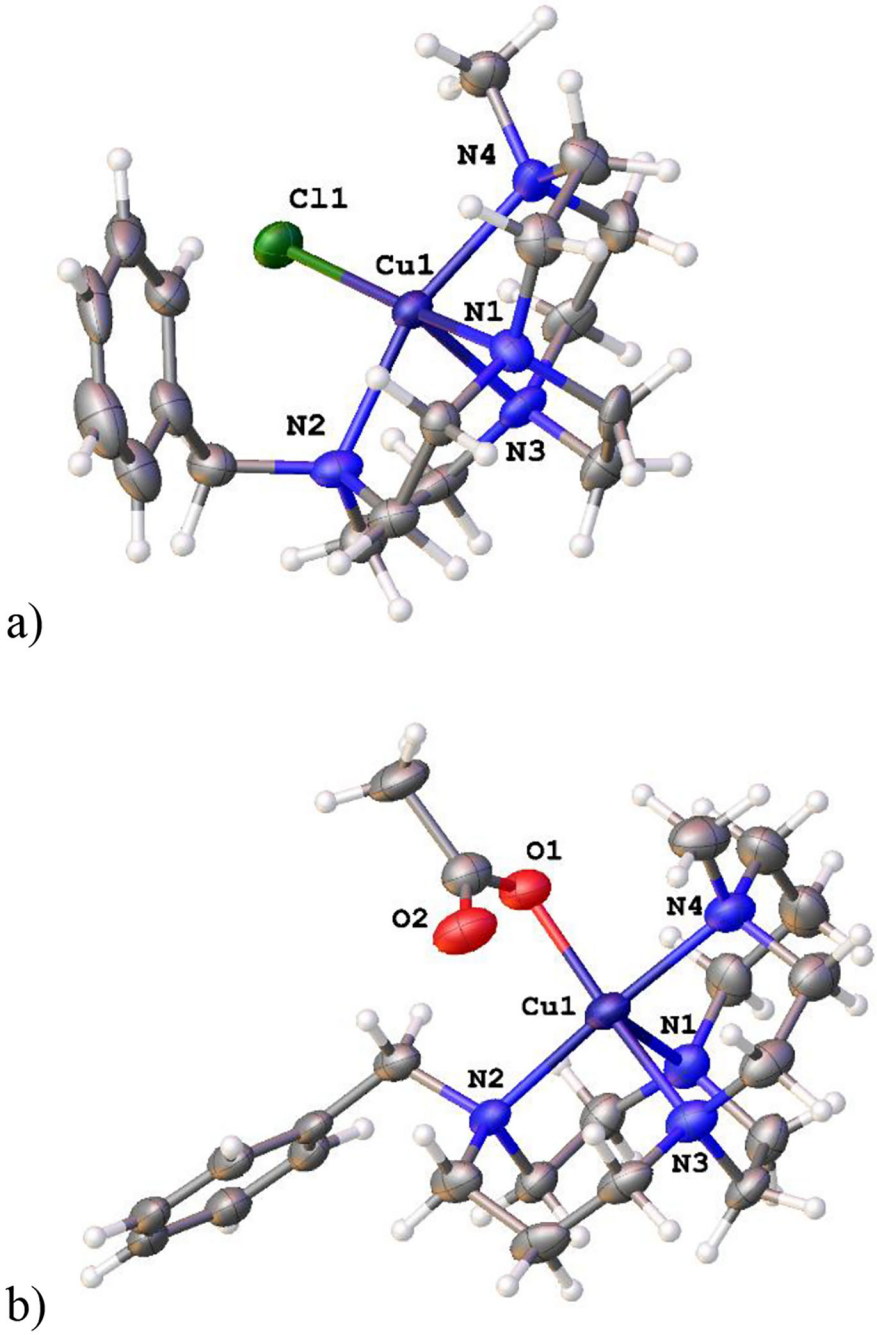

Figure 3.

The X-ray crystal structures of a) [Cu(**L1**)Cl]$^{+}$ (top) and [Cu(**L2**)(OAc)]$^{+}$[49] demonstrate the flexibility of the benzyl group, which can fold toward an empty coordination site as in [Cu(**L1**)Cl]$^{+}$ or away from a more sterically crowded metal ion as in [Cu(**L2**)(OAc)]$^{+}$.

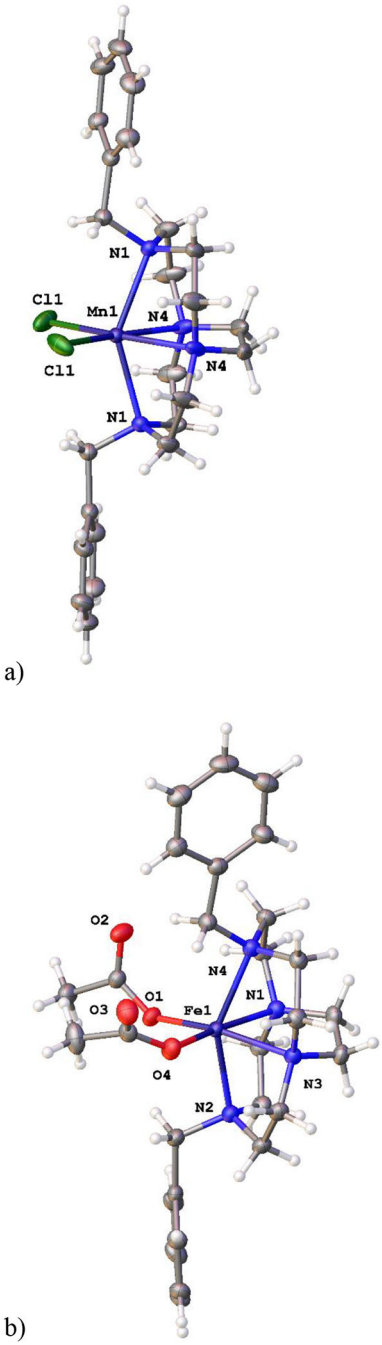

Figure 4.
The X-ray crystal structures of a) [Mn(**L3**)Cl_2] (left)[58] and b) [Fe(**L3**)$(OAc)_2$] (right).

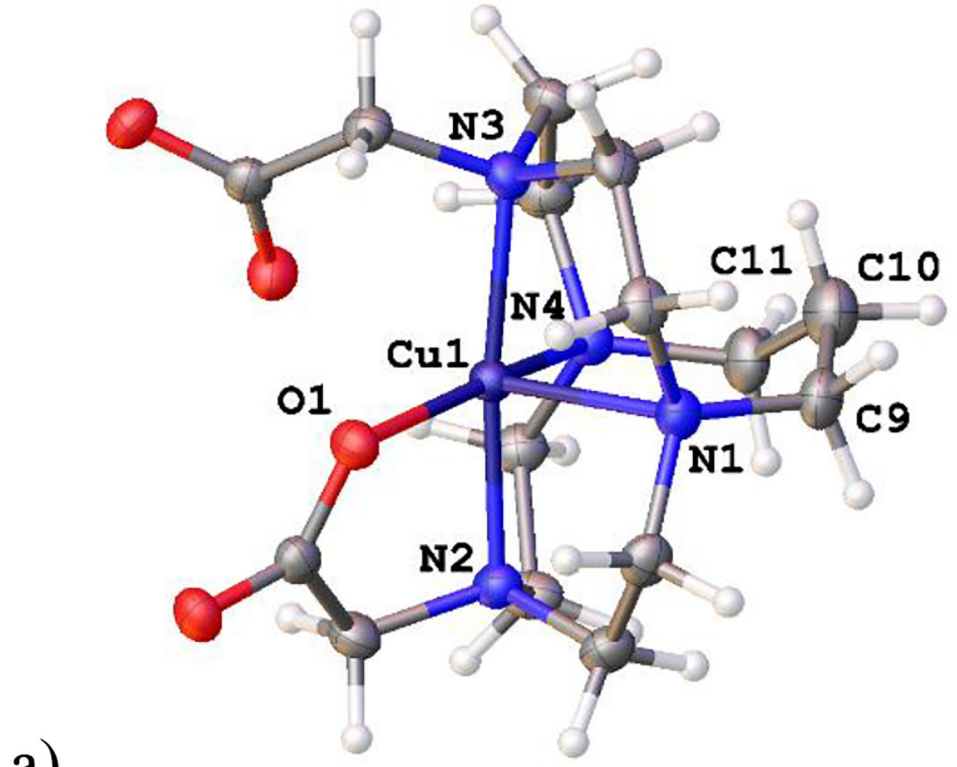

a)

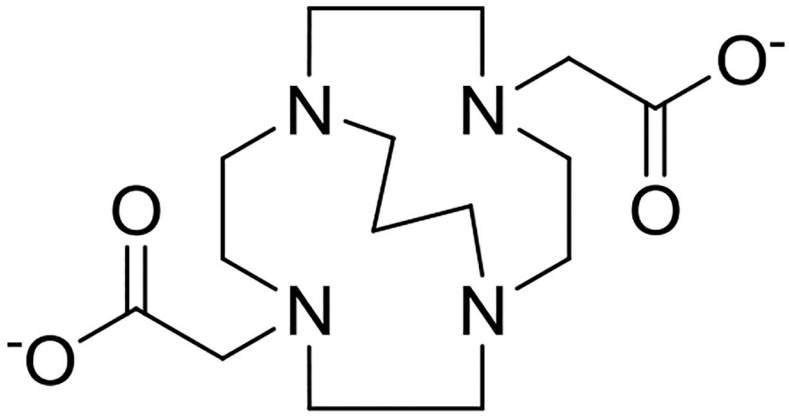

b) **CB3-DO2A**

Figure 5.
a) The X-ray crystal structure[61] of Cu(**CB3-DO2A**)$^{+}$ and b) the **CB3-DO2A** ligand

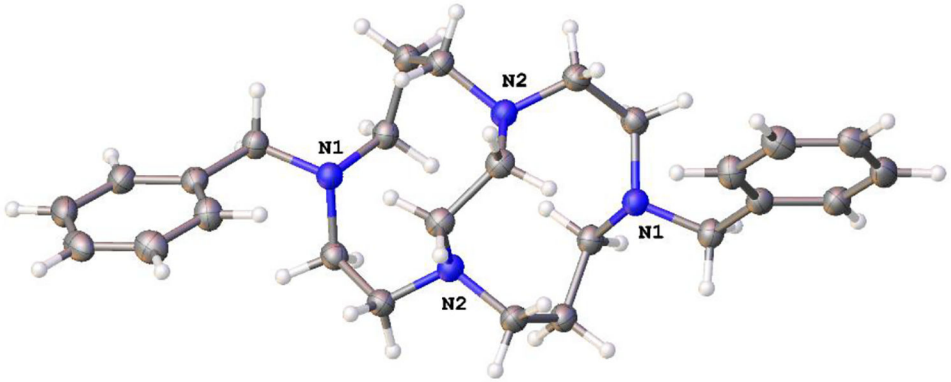

Figure 6.
The X-ray crystal structure of **L8**.

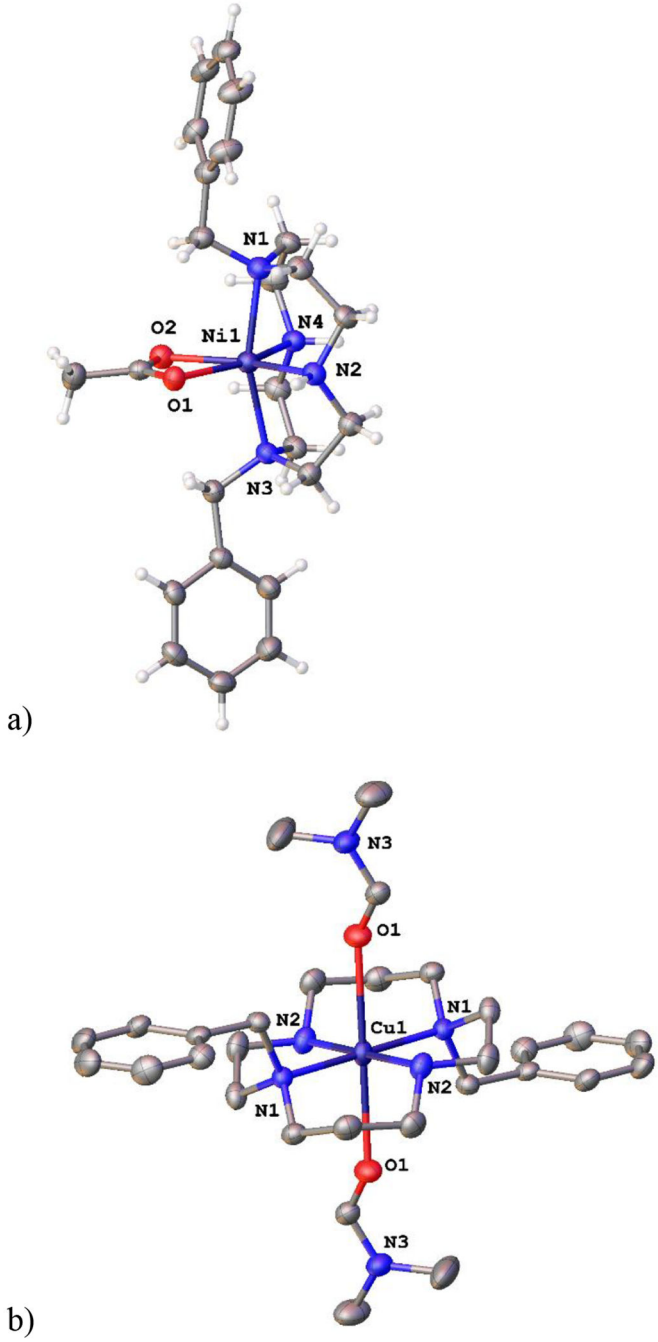

Figure 7.
The X-ray crystal structures of a) Ni(**L7**)$(OAc)^{+}$ (left) and b) Cu(**L10**)$(DMF)_2^{2+}$.

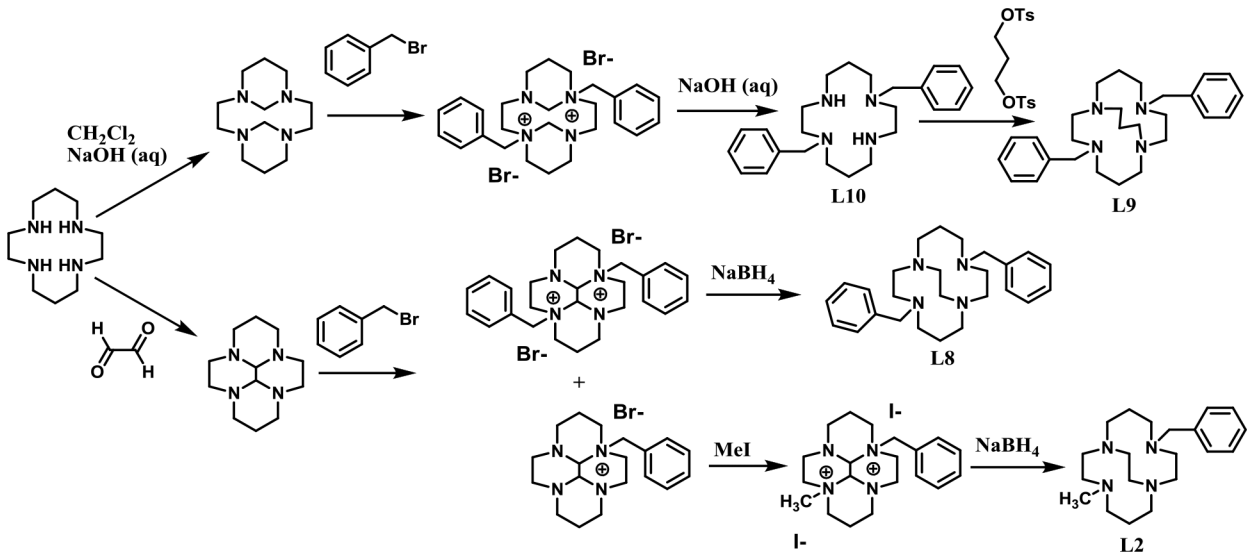

Scheme 1.

Synthetic scheme for the literature syntheses of cyclam ligands **L2**,[49] **L8**,[55] **L9**,[54] and **L10**.[53] Cyclen analogues **L1**,[51] **L3**,[55] **L4**,[56] and **L7**[57] are made by analogous reactions.

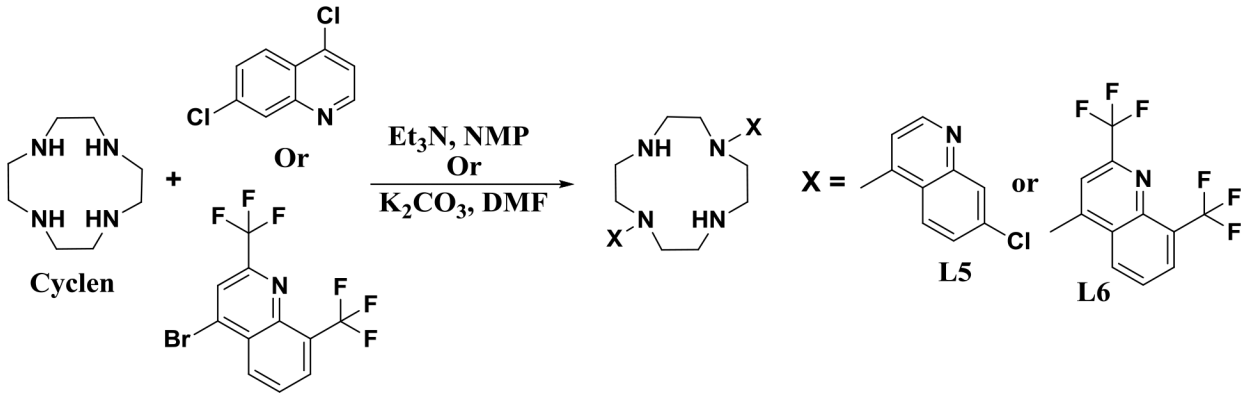

Scheme 2.

Synthetic scheme for the literature syntheses of cyclen bisquinoline ligands **L5**[39,47] and **L6**.[47]

Scheme 3.

Generic complexation reaction illustrated using **L2** and showing an acetate complex.

Table 1

The *in vitro* Inhibitory Activity of the Monocyclic Compounds against *L. donovani*.

Sample Code	*L. donavani* Promastigotes		*L. donavani* Amastigotes		*L. donavani* Amastigotes + THP1		THP1 cells (Cytotoxicity)	
	IC_{50} (μM)	IC_{90} (μM)	IC_{50} (μM)	IC_{90} (μM)	IC_{50} (μM)	IC_{90} (μM)	IC_{50} (μM)	IC_{90} (μM)
Pentamidine	2.93	6.52	20.42	>25	29.38	9.14	>20	>25
Amphotericine B	0.134	0.262	0.790	0.959	0.48	1.94	>10	>10
Bn_1Me_1Bcyclen (**L1**)	>20	>20	>20	>20	>20	>20	>20	>20
[Cu(**L1**)(OAc)]PF_6	>20	>20	>20	>20	>20	>20	>20	>20
[Zn(**L1**)(OAc)]PF_6	>20	>20	>20	>20	>20	>20	>20	>20
Bn_1Me_1Bcyclam (**L2**)	>20	>20	>20	>20	>20	>20	>20	>20
[Ni(**L2**)(OAc)]PF_6. 0.35NH_4PF_6	>20	>20	>20	>20	>20	>20	>20	>20
[Cu(**L2**)(OAc)]PF_6	>20	>20	>20	>20	>20	>20	>20	>20
[Zn(**L2**)OAc)]PF_6	>20	>20	>20	>20	>20	>20	>20	>20
Bn_2Bcyclen (**L3**)	12.68	11.44	15.14	22.29	>25	>25	>25	>25
Mn(**L3**)Cl_2	18.93	>20	11.50	17.09	>20	>20	>20	>20
[Fe(**L3**)(OAc)]PF_6	>20	>20	>20	>20	>20	>20	>20	>20
[Ni(**L3**)(OAc)]PF_6	10.95	>20	>20	>20	>20	>20	>20	>20
[Cu(**L3**)(OAc)]PF_6	>20	>20	>20	>20	>20	>20	>20	>20
[Zn(**L3**)(OAc)]PF_6	4.73	>20	13.64	>20	>20	>20	>20	>20
Bn_2PBCyclen (**L4**)	15.61	>20	>25	>25	18.24	>25	>25	>25
[Mn(**L4**)($C_2H_3O_2$)]PF_6. 1.9NH_4PF_6	>10	>10	>10	>10	>10	>10	>10	>10
[Fe(**L4**)($C_2H_3O_2$)]PF_6. 1.2NH_4PF_6	>20	>20	>10	>10	>10	>10	>10	>10
[Co(**L4**)($C_2H_3O_2$)]PF_6. DMF	20.66	>20	>10	>10	>10	>10	>10	>10
[Zn(**L4**)($C_2H_3O_2$)]PF_6 0.2DMF	22.92	>20	>10	>10	>10	>10	>10	>10
CNBQ (**L5**)	>20	>20	>20	>20	>20	>20	>20	>20
Mn(**L5**)Cl_2	7.40	11.46	>15	>15	8.59	10.99	13.20	>15
Fe(**L5**)Cl_2	4.13	7.07	>10	>10	3.52	5.24	3.95	8.79
Bis-BQ-Cyclen (**L6**)	>20	>20	>20	>20	>20	>20	>20	>20
Bn_2Cyclen (**L7**)	10.47	>20	>25	>25	-	2.8	>25	>25
Mn(**L7**)Cl_2	2.82	9.12	>20	>20	1.02	2.40	>20	>20
Fe(**L7**)Cl_2	5.50	13.09	>15	>15	1.89	6.56	>15	>15
Ni(**L7**)Cl_2. 3H_2O	18.63	>20	>20	>20	>20	>20	>20	>20
Bn_2Bcyclam (**L8**)	20.81	>20	>20	>20	10.06	10.43	>20	>20
Mn(**L8**)Cl_2	21.99	>20	>15	>15	>15	>15	14.27	>15
Fe(**L8**)Cl_2	7.80	20.09	>15	>15	>15	>15	>15	>15
[Co(**L8**)(OAc)]PF_6. H_2O	35.29	>20	>15	>15	>15	>15	>15	>15

Sample Code	*L. donavani* Promastigotes		*L. donavani* Amastigotes		*L. donavani* Amastigotes + THP1		THP1 cells (Cytotoxicity)	
	IC_{50} (μM)	IC_{90} (μM)	IC_{50} (μM)	IC_{90} (μM)	IC_{50} (μM)	IC_{90} (μM)	IC_{50} (μM)	IC_{90} (μM)
[Ni(**L8**)(OAc)]PF_6	6.51	>20	>15	>15	>15	>15	>15	>15
[Zn(**L8**)(OAc)]PF_6	4.73	>20	>15	>15	>15	>15	>15	>15
Bn_2PBCyclam (**L9**)	12.98	18.97	18.54	23.11	11.10	11.43	20.63	22.80
[Mn(**L9**)][$MnCl_4$]. CH_3CN	3.48	9.11	1.50	2.68	1.89	2.17	3.49	5.90
[Fe(**L9**)][$FeCl_4$]. H_2O	11.69	>20	10.14	>14	11.93	>14	>14	>14
[Co(**L9**)$(OAc)_{1.1}$]$(PF_6)_{0.9}$. DMF	7.98	>13	10.45	13.09	>13	>13	>13	>13
[Ni(**L9**)$(OAc)_{1.1}$]$(PF_6)_{0.9}$. DMF	9.33	>13	10.12	12.96	>13	>13	>13	>13
[Zn(**L9**)(OAc)]PF_6.0.3NH_4PF_6	8.17	10.50	9.91	13.48	7.81	8.53	>14	>14
Bn_2Cyclam (**L10**)	9.40	17.84	>25	>25	12.93	13.19	>25	>25
Mn(**L10**)Cl_2. H_2O	6.62	12.36	>19	>19	12.36	12.68	>19	>19
Fe(**L10**)Cl_2. 0.5 H_2O	5.64	13.91	>19	>15	9.61	9.68	>19	>19
[Co(**L10**)(OAc)](PF_6). H_2O	>15	>15	>15	>15	>15	>15	>15	>15
Cu(**L10**)(OAc)](PF_6). H_2O	>20	>20	>15	>15	>15	>15	>15	>15
[Zn(**L10**)(OAc)]PF_6. 0.1H_2O	5.65	11.28	>15	>15	6.80	7.04	>15	>15